MAGIC-TDAS 06-06
060630/Garczarczyk

Study of the focussing and mirror quality of the MAGIC reflector

Markus Garczarczyk	MPI München
Hans Anderhub	ETH Zürich
Adrian Biland	ETH Zürich
Francesco Dazzi	Università di Padova

June 2006

Abstract

After the recent AMC maintenance and refocussing we would like to show the results of measurements related with the focussing and single mirror quality. The different measurements were performed during the last half an year. This internal note covers results of the PSF and reflectivity of the MAGIC reflector. In addition aberration effects for off-axis pointing are compared with numerical ray tracing results showing very good agreement. In the end new focussing methods using star images are described and further improvements of the AMC behavior are shown. Finally we also include an short summary of the single mirror replacement which has been performed September last year.

1 Mirror quality and PSF measurements

1.1 PSF long time stability

PSF measurements with the SBIG camera

The last focussing has been performed end of September 2005, almost half an year ago. We have learned in former time that the laser focussing do not give constant focussing quality. It shows more an linear degradation versus the time. Since the source of this degradation is not known yet[1], we have decided to switch to LUT focussing as standard focussing method during observations. Figure 1 shows PSF measurements performed with the SBIG camera, pointing and focussing the telescope at different stars. In the time window shown in this figure, two Roque lamp focussing had been performed. The first focussing was in September 2005 and the second now in April 2006. Two different focussing methods are shown: PSF after laser- and after LUT focussing. It is clearly visible that the resulting PSF with lasers show linear degradation with time (it is indicated with the red line). The LUT focussing stays astonishingly constant in this time period. Weather conditions, specially mirror dish extension due to varying temperatures, could be the reason for small variations. We did not correlate zenith dependent differences of the PSF, which shown in chapter 1.5, could have an effect of ∼4 mm for different zenith positions.

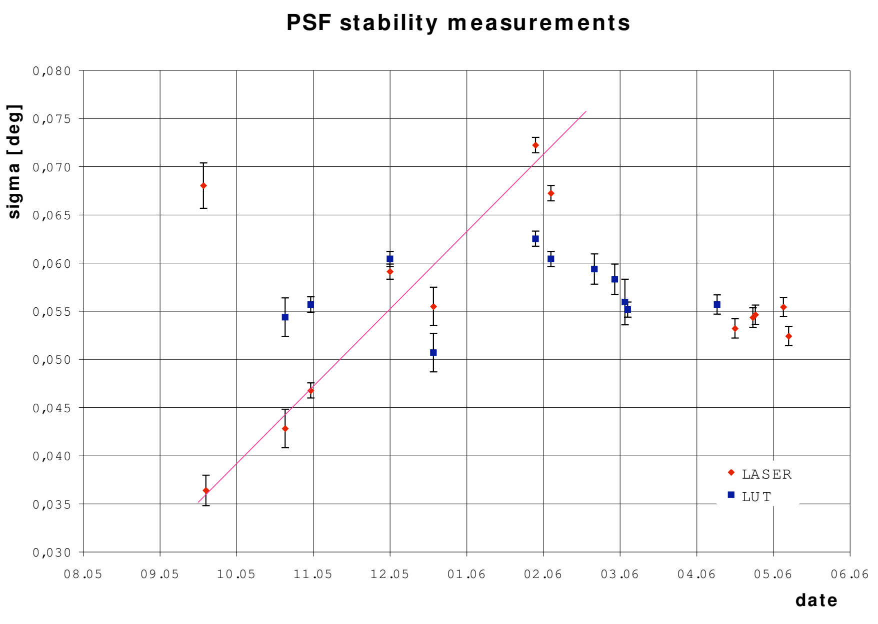

Figure 1: PSF measurements with the SBIG camera covering the time between September 2005 and May 2006. Red points are measurements after laser focussing and blue dots after LUT focussing. Most of the points include more than one PSF measurement. The error bars include the spread of the results. During this time period LUTs were used as standard focussing method during observations.

[1]Since beginning May 2006, a long time stability test with eight laser modules is performed in the MPI.

PSF results from the muon analysis

The advantage of good parametrisation of the muon rings observed by IACT and their general character allow to extract the PSF of the telescope reflector using their shower images. This is done by comparing the width of the ring with MC simulated muons reflected at a reflector characterized by different PSF. Detailed description of the method can be found in [1, 2].

Figure 2 shows the results from the muon ring analysis for the time period between September 2005 and April 2006 [3], the same period as shown in previous plot. An improvement of the PSF in October 2005 after the refocussing with the Roque lamp can be seen. Since November 2005, when new LUTs were generated and used as standard focussing procedure during observations, the PSF stayed constant $<\sigma>= 0.052°$. This value is comparable with the results from the SBIG measurements when taking into account that the PSF of a star image at the spectralon plate is not in the optimal focus; The PSF with muon rings detected in the PMT plane should show better values, as it is the case.

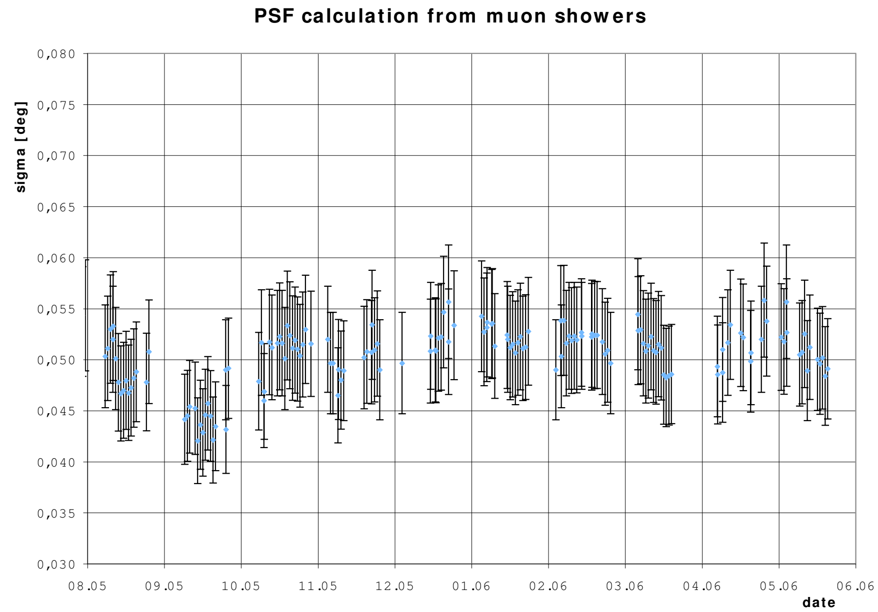

Figure 2: Long time behavior of the PSF determined with the broadening of the muon ring images extracted from the data of MAGIC telescope. Each point represents the mean of the day averaged PSF from the complete data sample. The error bars represent the 20% error for the method.

1.2 Detailed PSF measurement results

In addition to figure 1, few selected PSF plots are shown in figure 3. The first image shows the focussed image of Alderamin, taken on 22^{nd} October, 2005, before Roque lamp focussing. The second image shows the best PSF achieved up to now. The image shows Andromeda Gamma (Almach), taken on 23^{rd} October 2005, just after the new focussing. The two spots in the right upper- and lower corner are neighbor stars. The third image is taken on 11^{th} April, 2006, one day before the last Roque lamp focussing. The tail shows individual spots from disabled, not working panels. The actuators of this panels were repaired and the last picture in figure 3 shows the PSF from 7^{th} May, 2006. Detailed results of the PSF measurement are summarized in table 1.

The radius with 80% of the light content r_{80} was determined from the two dimensional light distribution by summing up the ADC values for the CCD pixels in circles around the spot maximum. The conversion to the two dimensional σ can be computed with the following formula:

$$r_{80} = \sqrt{\ln 5} \cdot \sigma \tag{1}$$

date	star	exposure time	focussing	$r_{80} [mm]$	σ [mm]
22.09.2005	Alderamin	20 sec	laser	27.5	21.7
23.09.2005	Andromeda Gamma	20 sec	laser	13.3	10.5
11.04.2006	Regulus	8 sec	LUT	18.5	14.6
07.05.2006	Polaris	5 sec	laser	20.8	16.4

Table 1: Selected results from the PSF measurements with the SBIG camera.

1.3 Quality of individual panels

Recently, in parallel to the Roque lamp focussing, high resolution images of individual panels have been taken. The individual spots are shown in figure 4, aligned in the shape of the MAGIC reflector dish. Figure 5 (top) shows the integrated light content of each panel, normalized to the panel with the highest value. Out of this figure the quality of individual panels can be compared among the others. To make such a comparison three correction factors have been included:

- The panels assembled with only three mirrors instead of four (panels at the four inclined edges of the telescope dish as well as few panels close to the elevation axis) are normalized to the others (by factor 1.33).
- Due to the parabolic shape of the reflector dish panels away from the center are inclined to the parallel beam of light. This reduces the mirror area of the outer panels and have to be corrected. The correction factor f_{area} is in the first order approximation only dependent

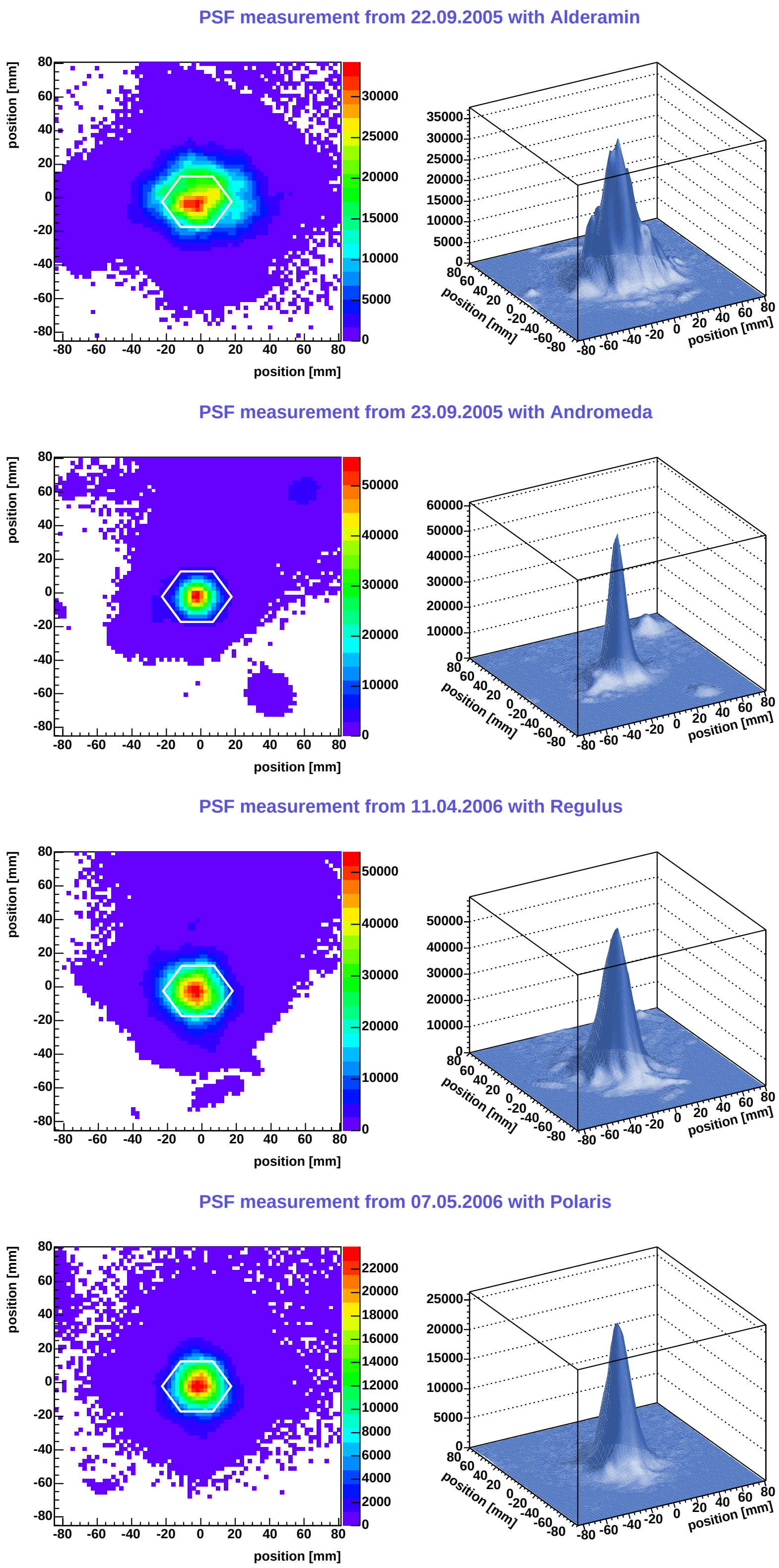

Figure 3: Selected images of the PSF taken in the last half an year. The corresponding results are shown in table 1.

on the distance r of the panel to the dish center:

$$f_{area} = \frac{\sqrt{(\frac{r}{2})^2 + 17^2}}{17} \tag{2}$$

- The measurement span over two nights and the spots have shown lower light content for the second night which could be due to different alignment of the lamp or moonlight conditions. The mean of the panels in the five upper rows are therefore normalized to the mean of the panels in the lower five rows.

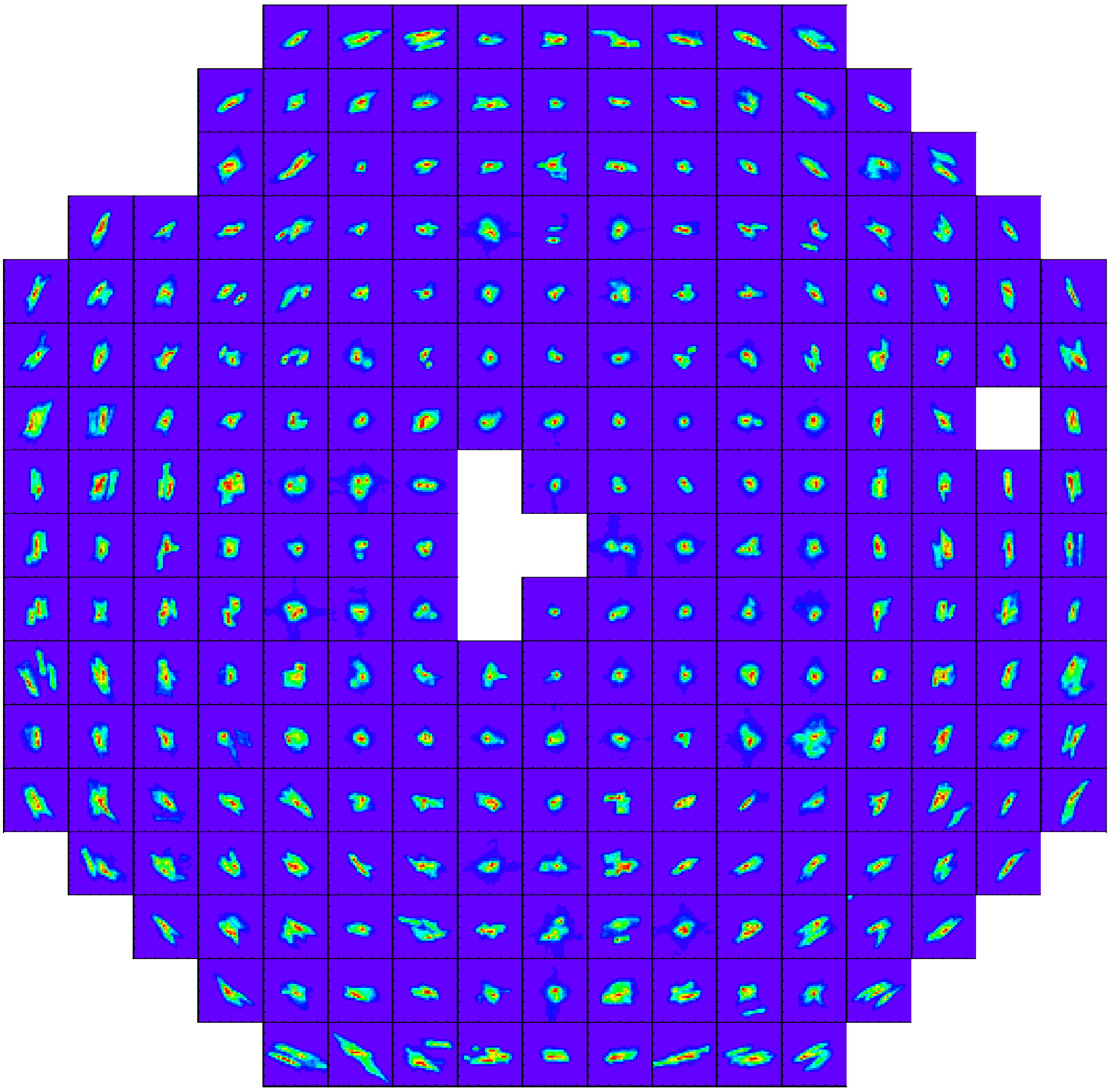

Figure 4: Reflected spot shape for individual panels mounted at the telescope dish. The six white placeholders inside the structure are either due to missing images or due to missing panels (two central panels). Each individual image has the border size of 70 mm. The elongated spots at the outer part of the telescope dish are caused due to aberration effects. There are few panels where the single mirrors do not exactly overlap – clearly separated spots.

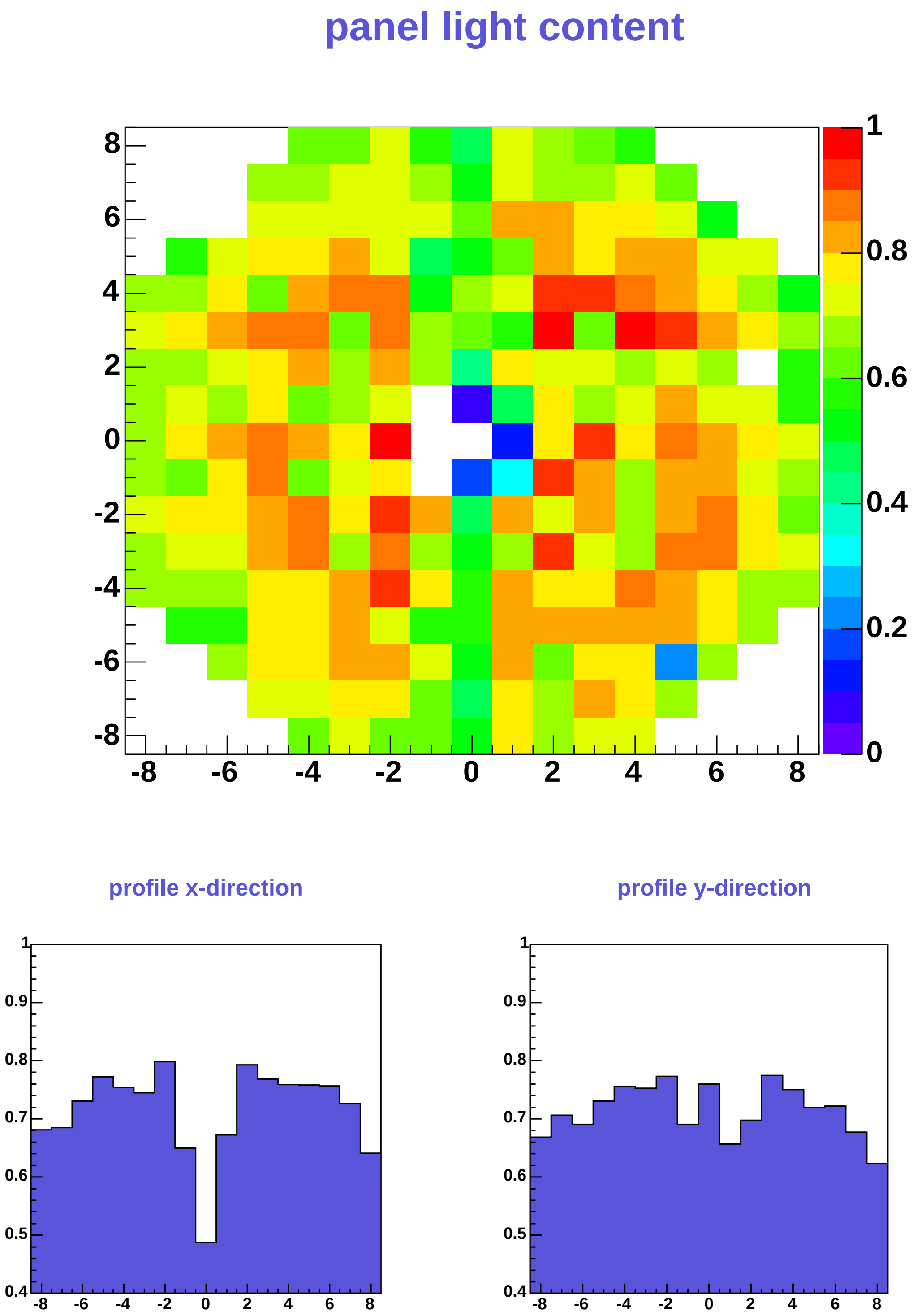

Figure 5: *Top:* Integrated light content of each individual panel. The background is subtracted from the images. The individual integrals are normalized to the panel with highest value. The central panels along the y-axis and the panels directly in the center are partially shadowed by the camera bowl and the camera itself. This panels have therefore less light content than the others. *Bottom:* Profile of the integrated light content in x- and y- direction along the telescope dish.

1.4 Prototypes of one square meter mirrors

End of November 2005 four new, one square meter mirrors were installed on the telescope dish. This mirrors are prototypes for the MAGIC-2 telescope and have to be tested first under real weather conditions at the MAGIC site. In the figure 4 and 5 the three *Padova-design* mirrors are included. The coordinates at the telescope dish are (2,-4), (3,-4) and (4,-3). There is one additional mirror of the *MPI-design* placed at (-1,-1). Unfortunately we did not made any picture of this panel during the Roque lamp focussing. This panel has been mounted in the wrong place in November and we succeeded to exchange the position only after the focussing.

Figure 6 shows the comparison of the three *Padova-design* mirrors. While two of the mirrors show only aberration effects and no significant degradation, the panel (4,-3) shows big worsening of the optical spot. In addition, the reflectivity of the new panels – in comparison to the direct neighbors – is lower by 8% for (2,-4) and (3,-4) and by 18% for the panel (4,-3) (see figure 5).

1.5 Optimal focal length setting for the Winston cones

It is important to know the optimal focal length for the Winston cone plane of the PMTs. We have measured the distance between the front of the spectalon plate and the front of the winston cones. For this measurement the plexiglas window of the PMT camera had to be dismounted. The distances are shown in figure 7. According to our measurement the distance described above is 46 $\pm$ 2 mm. The error is due to possible play of the camera lid. The camera body was positioned after the Roque lamp focussing in the way, that the front side of the camera body has 65.0 mm distance to the front plane where the bellows is mounted. The position at the rulers mounted at the rails of the camera body are (viewed from the back side of the PMT camera):

- top left: 26.0 mm
- top right (ruler missing, distance from the pointer till the front of the rail): 27.4 mm
- bottom left: 26.0 mm
- bottom right: 25.8 mm

Now, the optimal focal length which gives best PSF at the Spectralon plate has to be determined. Two measurements had been performed. One measurement close to the zenith (Alphecca) and the other one with Polaris at 63° zenith angle. The results are shown in figure 8. The best PSF is in the minimum of the fit. The minimum for Zenith lies at $a = -0.8$ mm and for large zenith angles at $a = -4.6$ mm, where a (x-axis in figure 8) is the correction to the standard focal length setting in the AMC. From this measurement one can also estimate the gravitational camera sagging to be **3.8 mm** at zenith, which is in good agreement with the measured value using the DISTO laser distance measurement device.

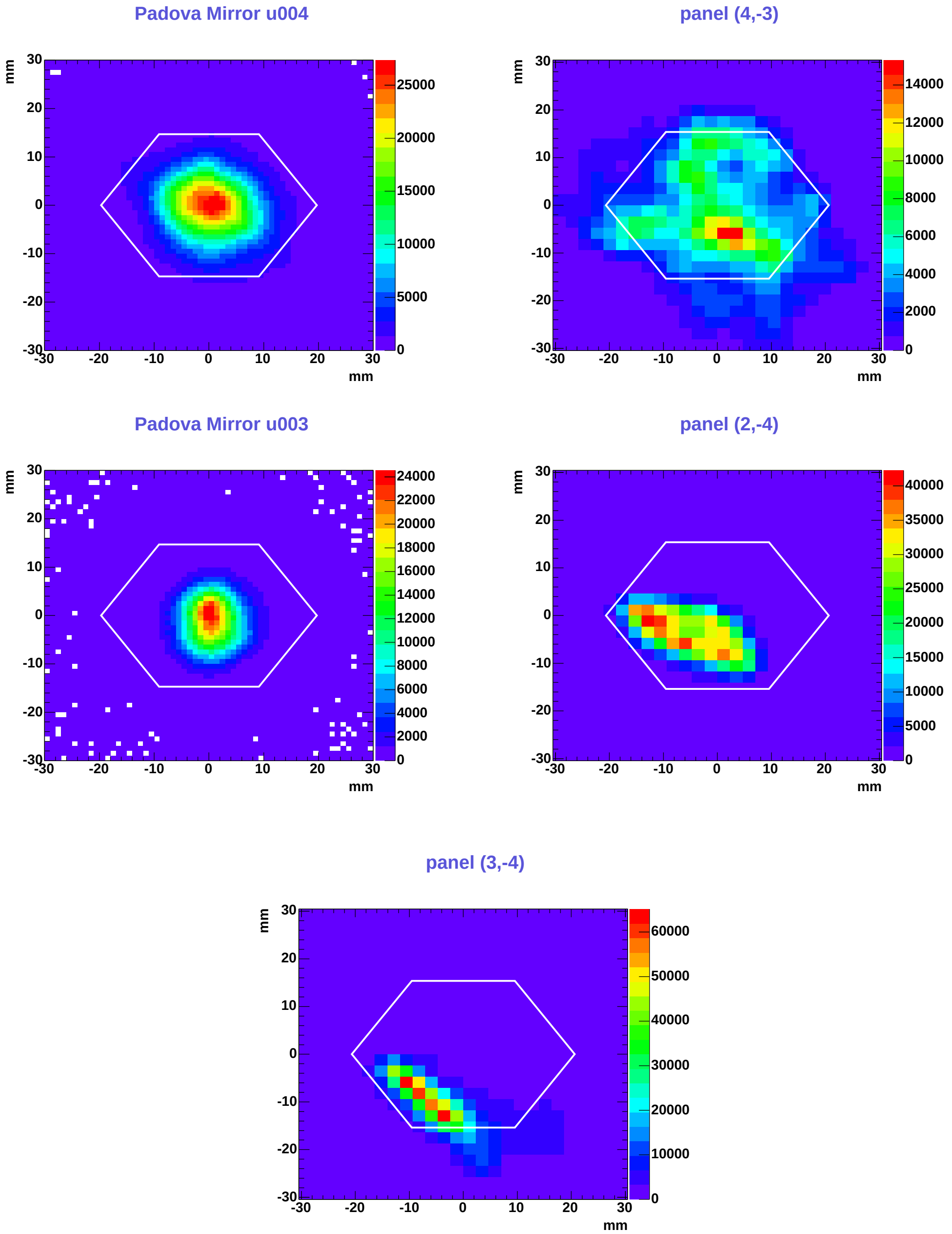

Figure 6: Mirror quality of the novel one square meter mirrors after after 1/2 year telescope dish experience. On the *left side* the mirror spot just after the diamond milling is shown. The *right side* shows the same mirror measured at the telescope, 1/2 year after the installation. One have to take into account that the mirrors on the right side are blurred due to aberration effects while the figure on the left side was taken with the panel perpendicular to the light beam. For the panel (3,-4) no image measured after the diamond milling could be found. The size of the central Winston cone is shown for comparison.

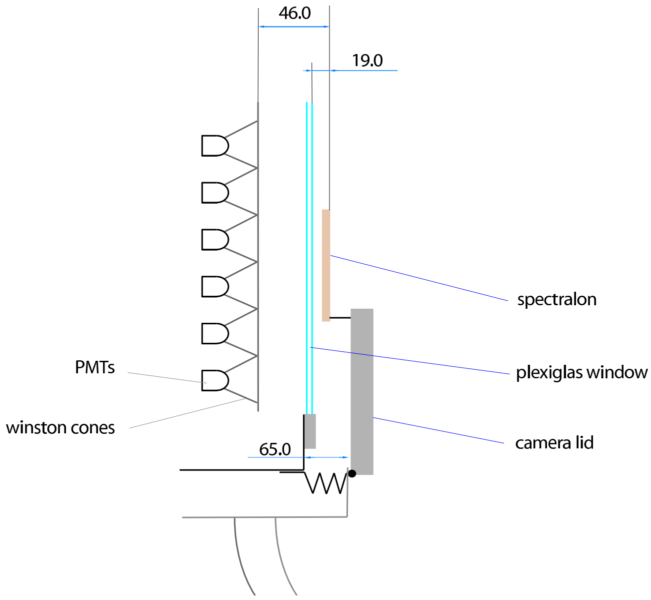

Figure 7: Distances measured at the MAGIC PMT camera.

The focal length correction factor in the AMC software should than be set to:

- for zenith: $a_{current}$ + 47 mm - 30 mm
- for high zenith angle $\sim 90°$: $a_{current}$ + 51 mm - 30 mm

By subtracting 30 mm one archives the best focus for 10 km distance.

1.6 Focussing of the MAGIC mirrors with the SBIG camera and star images

The very sensitive SBIG camera allows to record the reflected image of an single mirror from a star. This makes it suitable for focussing the MAGIC reflector with stars within appropriate time. This method have three main advantages:

- Other experiments at the observatory are not disturbed by the artificial light source.
- The MAGIC PMT camera has not to be displaced to compensate the focal length correction; One needs to shift the camera by 290 mm to correct between light source at infinity and a corresponding one at 980 m.
- In principle any bright star (mag >2) can be used for the refocussing.

Polaris has the advantage that it stays $\sim$ in the same zenith position and no big variations of dish deformation are expected during the focussing time. On the other hand the Spectralon plate is directly illuminated by the moonlight witch can be partially reduced using an shadowing cone mounted on the camera lid.

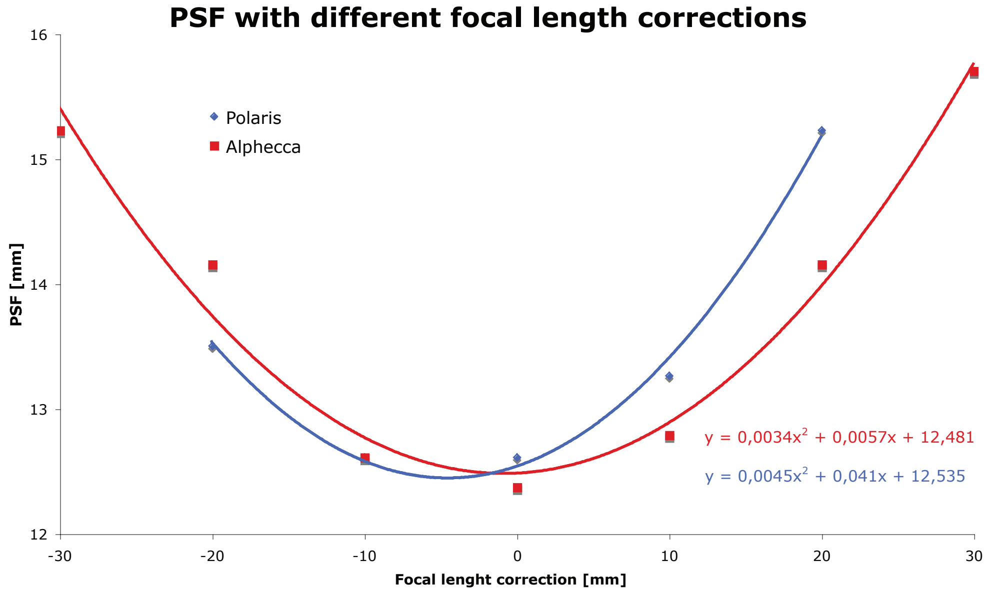

Figure 8: PSF measurements with different corrections of the focal length.

2 Aberration effects by off-axis pointing

2.1 Short introduction to aberrations

In an ideal optical system, all rays of light from a point in the object plane would converge to the same point in the image plane, forming an clear image. The influences which cause different rays to converge to different points and blur the image are called **aberrations**. There are many types of aberrations categorized into 1st order, 3rd order, 5th order etc. The most common types are the 3rd order aberrations.

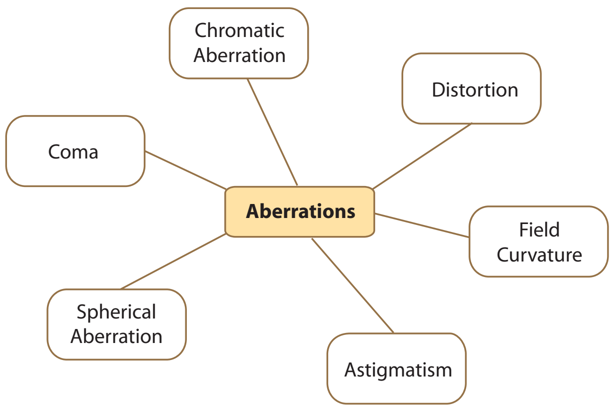

Figure 9: Different aberration types.

The 3rd order aberrations are classified in six types as shown in figure 9. All, except the **chromatic aberration** affect both, the refracting and reflecting telescopes; The chromatic aberration affects only refracting telescopes.

The **spherical aberration** plays an role for spherical mirrors and lenses. Rays parallel to the optical axis, striking the mirror surface at different distances from the center, are focussed at different focal lengths.

The **curvature of field** occurs when the image if focussed on a curved plane. The production of a curved camera plane for IACTs is unrealistic and one needs to accept the aberration.

The **distortion** shifts the image position. The images of lines that meet directly in the origin appear straight, but the images of any surrounding straight lines appear curved. There are two types of distortion: *pincushion* and *barrel*. Optical systems without aperture, e.g. the MAGIC reflector, are free of distortion and are called *orthoscopic*.

For large reflectors the **astigmatism aberration** becomes important. This aberration is caused due to the fact, that the focal length along one diameter differs from that along the another. Instead of focussing rays to a point, they meet it two line segments perpendicular to each other. These are the sagittal and tangential focal lines. Even when the overall reflector geometry of MAGIC has parabolic shape, the single mirrors are spherical approximation of the surface. The sum of the spherical- and astigmatism aberration as well as field curvature cause blurred and elongated spots by single mirrors depending on their off-axis position from the center of the dish (see figure 4). The optimal focussing power is reached by mirrors with the same radius of curvature of the paraboloid which is the case for the central area. Far from the center of the dish, the difference between the shape of the paraboloid and the spherical mirrors increases and the dimensions of the spot too.

Coma aberration is an inherent property of telescopes using parabolic mirrors. Light from a point source (such as a star) in the center of the field is perfectly focussed at the focal point of the mirror. However, when the light source is off-axis, the different parts of the mirror do not reflect the light to the same point. This results for a point of light that is not in the center of the filed looking wedge-shaped. The further off-axis, the worse is this effect. Off-axis Stars appear to have a cometary coma, hence the name of the aberration. The Cherenkov photons generated in particle showers are emitted preferable in the path direction of the primary particle, however, specially for hadron showers the deviation to the optical axis becomes significant and makes the coma aberration as an important impact for the analysis of the image parameters. The impact of the coma aberration is simulated in the MC data. It can also be shown directly by observing an star misplaced to the optical axis. This measurement was performed with the SBIG camera and the comparison between the measured- and simulated PSF, at different distances to the star, are shown in the next chapter.

2.2 Influence of coma- and astigmatism aberration on the PSF

To understand the coma aberration we have compared results of the numerical ray-tracing with images taken from a bright star (Vega) by increasing the distance of the star to the optical axis of the telescope.

The simulation calculates the intersection point between the reflected light and the detector focal plane. In the ray-tracing a parallel beam of light inclined with the angle Θ to the optical axis of the telescope is simulated. The reflector describes the nominal shape of the MAGIC telescope: The overall reflector is following a paraboloid reproducing the MAGIC dimensions. It is composed of 964 spherical mirror segments with the size 500×500 mm^2. The radius of curvature for each individual mirror is set to its nominal value. The single mirror axis is perpendicular to the paraboloid surface on the central point of the mirror – it represents a perfect alignment of the system. One photon per two cm^2 incises the surface.

Widening of the PSF with increased inclination angle Θ to the optical axis is predicted. The effect is indeed observed and shown in figure 10; The aberrations cause an asymmetric tail away from the optical axis. A more quantitative description of the spot shape is provided by projections of the intensity distribution on the radial and tangential directions, shown in figure 11 for angles of 0°, 0.8° and 1.5° relative to the optical axis.

The comparison between the simulation and the measurement is done by comparing r_{80} – the radius with 80% of the light content. The radius is determined from the radial- and tangential projections of the PSF. The radial axis goes from the camera center to the spot and the tangential axis is the corresponding orthogonal direction. The measurements demonstrate that the spot width depends primary on Θ. With increasing angle to the optical axis the spot width increases, following a second order polynomial function. The results are included in figure 12. The simulated PSF is slightly better than the measured one. Taking into account that the ray-tracing simulation is based on ideal optical performance: parabolic shape of the reflector, spherical mirror segments with ideal radii of curvature and ideal alignment of the mirrors, this can be explained. However, both lines are within the MAGIC camera FOV parallel to each other, indicating once more that the measurement is in good agreement with the numerical simulation.

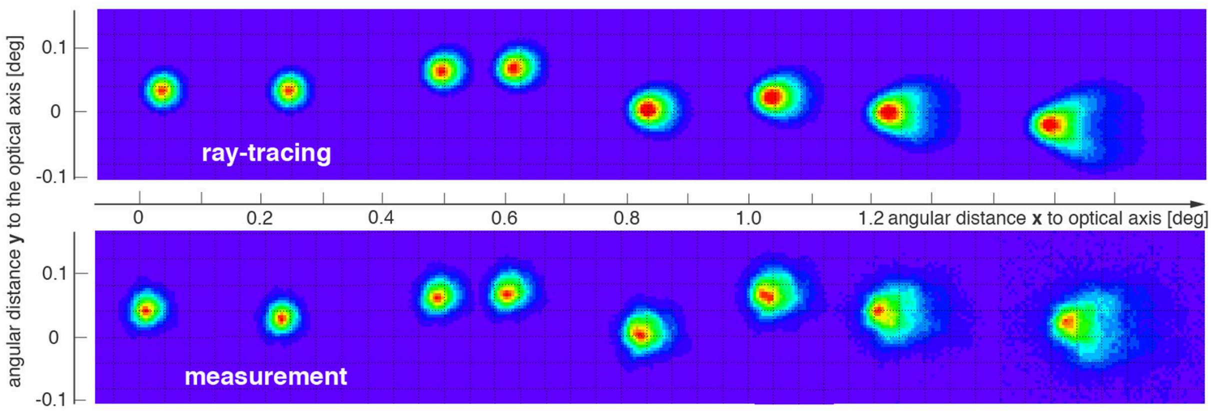

Figure 10: Comparison of the measured (bottom) and simulated (top) PSF with varying off-axis angle Θ. With increasing radial distance from the camera center the comet-like PSF becomes pronounced. The simulation was performed for the corresponding x- and y- distance to the camera center determined with the starguider LEDs.

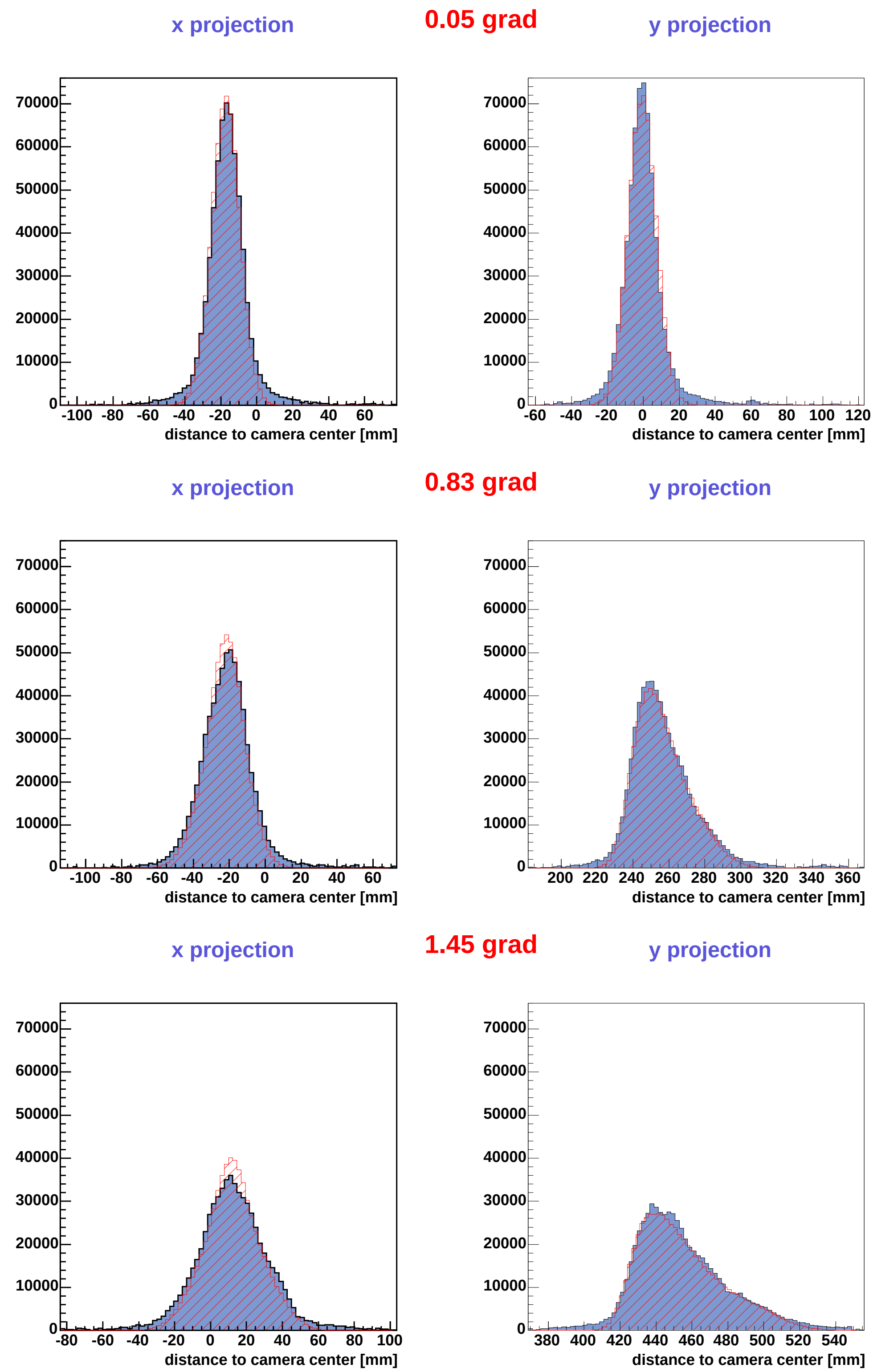

Figure 11: Radial and tangential projections of the PSF at different off-axis angles Θ. The blue area represents the measurement, the red shadowed area is the result of the ray-racing simulation. Comparing the on-axis view (upper plot at 0.05°), larger tales for the measured PSF are visible in respect to the simulated PSF – which represents an ideal gaussian distribution. The histograms are not normalized, therefore the simulation shows very good agreement with the measured PSF.

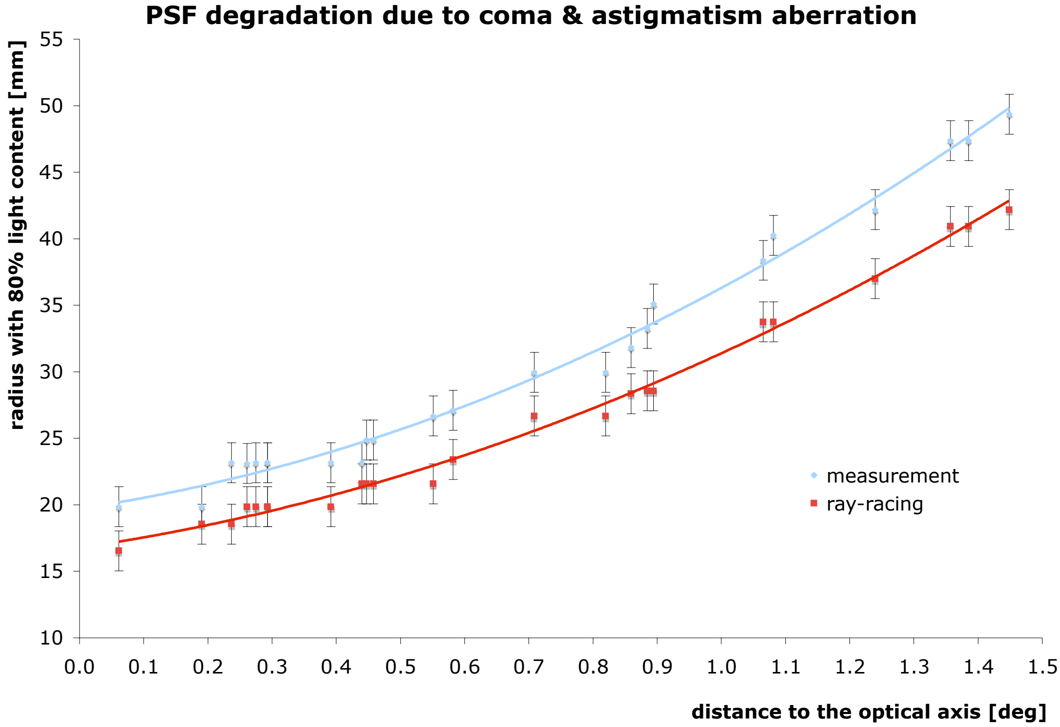

Figure 12: PSF degradation due to the influence of coma- and astigmatism aberration for off-axis pointing. Results from star measurement (blue) and numerical ray-tracing simulation (red) show good agreement by considering slight worser measurement than the ideal PSF simulation.

3 Reflectivity of the MAGIC reflector

The mirror reflectivity is important parameter in the performance of an IACT. It has a direct impact on the absolute scale of measured energy as well as on the flux of gamma rays from sources. In addition, the mirror reflectivity plays a role in the determination of the energy threshold of an IACT. The latter is inversely proportional to the quantity (mirror reflectivity $\times$ mirror area) [4].

We have developed a simple method to measure the reflectivity of telescope reflectors. While it is relatively easy to measure the reflectivity of the mirror material locally, it is not so straightforward to measure the amount of light they focus in a given spot. The method is based on the use of the SBIG camera, able to see simultaneously part of the telescope's focal plane and the sky region along the optical axis. The reflectivity measurement can be done in parallel to the PSF measurement, by pointing the telescope to a star. The ratio of the integrated scattered starlight from the spectralon plate $I_{\text{reflected}}$ to the integrated direct star spot I_{direct} provides a precise result of the product of (mirror area $\times$ mirror reflectivity). It is given by the formula:

$$R_{\text{mirror}} \times A_{\text{mirror}} = \frac{I_{\text{reflected}}}{I_{\text{direct}}} \cdot \frac{\pi \cdot d^2}{\cos \alpha} \cdot \frac{1}{R_{\text{diffuser}}} \tag{3}$$

where I_i are the luminosity integrated in ADC counts from the CCD image, R_{diffuser} is the reflectivity of the diffuser placed in the focal plane, α is the angle between the normal of the diffuser plate and the line connecting the CCD lens and d the distance between the plate and the camera lens.

Formula 3 is strongly dependent on the diffuser reflectivity and reflection characteristics. In our case a plate made of polytetrafluorethylene (PTFE) is used. The PTFE powder is pressed with 525 kPa in a form and sintered at 375° C [5]. The material has equal characteristics like Spectralon[2] with reflectivity higher then 99% for wavelengths from 400 to 1500 nm and almost perfect lambertian surface, scattering the light by a cosine intensity relationship $I(\Theta) = I(0) \cdot \cos\Theta$, where Θ is the incidence angle from the surface normal and $I(0)$ the incoming light intensity. Spectralon is used as a reference standard in many optical applications.

Before integrating the ADC counts from the reflected- and direct spot, the pedestal has to be removed. This is done by fitting an gaussian to the statistical distributed background and subtracting the mean from all CCD pixels. The integral is than calculated by summing-up all pixels with charge $\geqslant$ mean $+ 3\sigma$. Figure 13 shows the direct star image (left) and the reflected spot at the spectralon plate (right) of a second magnitude star with 10 sec exposure time. Because of the focusing at the 17 m distant MAGIC camera the star image at ∞ is smeared out which allows longer exposure time and better signal/noise ratios. The quantities $\alpha = 4.69 \pm 0.03°$, $d = 17045 \pm 3$mm and $R_{\text{diffuser}} = 98 \pm 1\%$ have been measured. By assuming the effective mirror area of $A_{\text{mirror}} = 230\,\text{m}^2$ with 2.5% shadowed part due to the camera bowl, wires and the camera itself, we obtained preliminary effective reflectivity values R_{eff} for the MAGIC telescope as shown in table 3. The optical filters (see figure 14[3]) mounted inside the camera filter reel allow to measure differential reflectivity's.

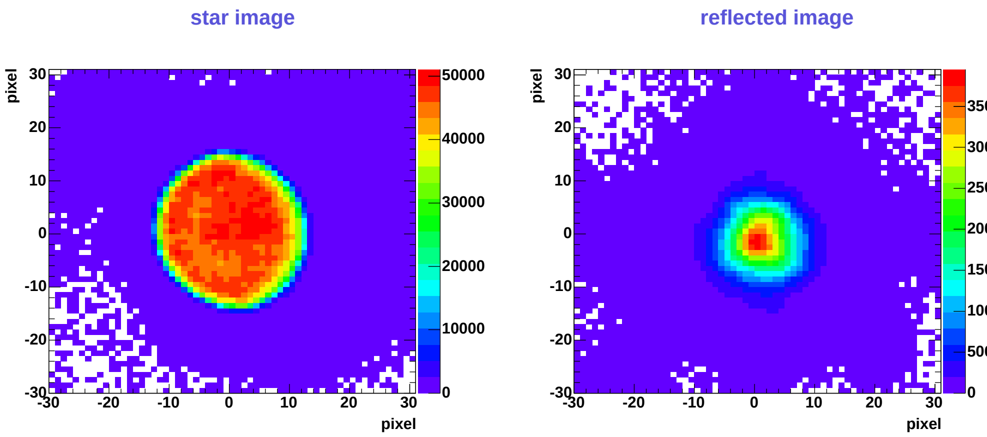

Figure 13: Examples of reflectivity measurement performed with the SBIG camera. *Left:* Direct star. *Right:* Reflected spot at the spectralon plate. *Note*: due to the high dynamic range of the camera the star image is still not saturated (16 bits $\hat{=}$ 65536).

[2]`http://www.labsphere.com`
[3]`http://www.sbig.com`

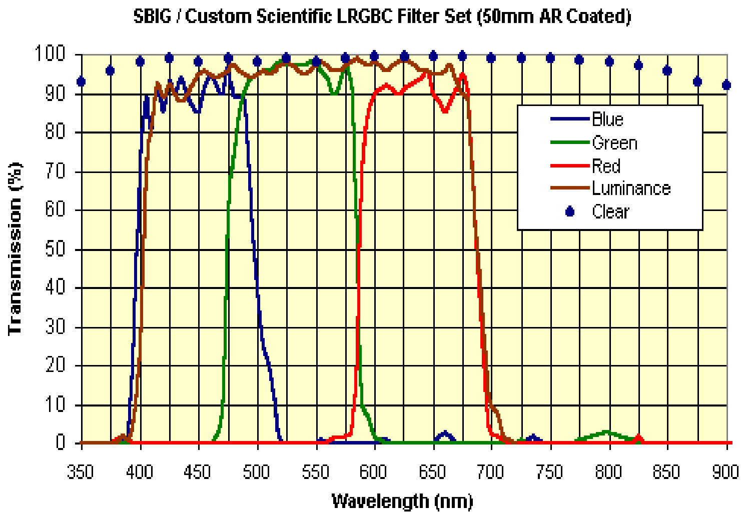

Figure 14: Transmission characteristics of the five optical filters mounted in the filter reel of the SBIG camera.

filter	wavelength [nm]	Reflectivity [%]	
		Alphecca	Dubhe
clear	–	80.4	80.5
luminance	380 - 700	82.5	85.2
blue	380 - 520	81.0	82.1
green	430 - 580	84.3	84.7
red	580 - 700	81.0	81.8

Table 2: Preliminary results for the effective reflectivity R_{eff} of the MAGIC reflector obtained from the SBIG image analysis. The error is $\pm 2\%$.

As already mentioned, reflector reflectivity can be calculated from the images taken during the PSF measurement, as long as the direct star image is not saturated. Figure 15 shows the results for the last half year. Since the effective mirror area is needed in formula 3 the values are also shown in the plot. The mirror area can be estimated from the log files of the AMC by checking the number of panels which have not been in operation during the focussing. The reflectivity do not show significant degradation over the last half a year. Fluctuations are direct measurement of the mirror surface cleanness.

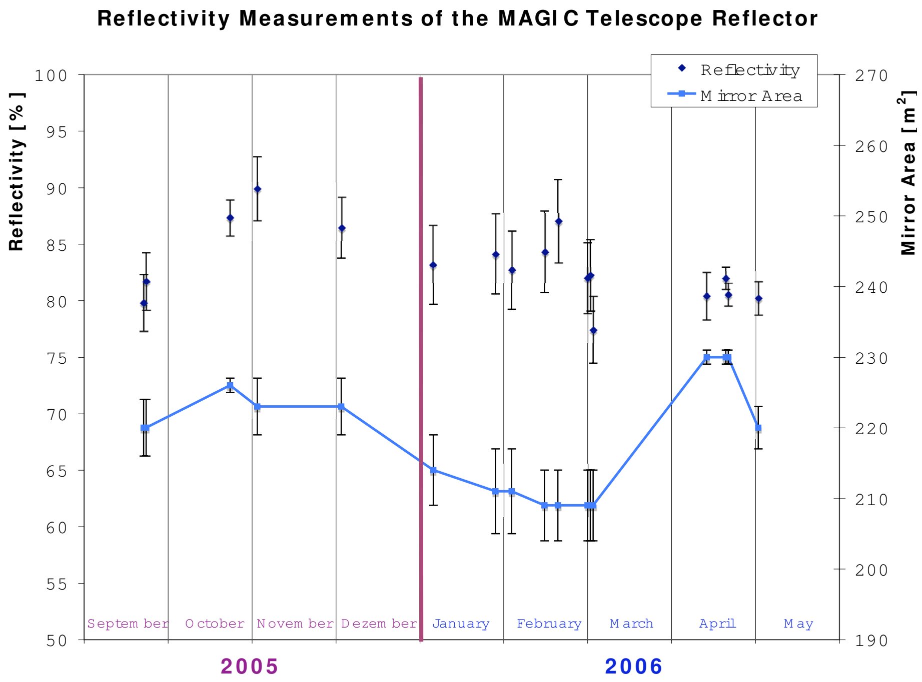

Figure 15: Effective reflectivity measured in the time period between August 2005 and May 2006. The values are determined from the PSF measurements, without any optical filter. In addition the effective mirror area is shown. The mirror area depends on the number of focussed mirrors during the measurement. This number is estimated from the AMC logfiles.

4 Status of the mirrors

In October 2005 we had an major mirror exchange at the MAGIC telescope. That time 41 single mirror segments have been successfully exchanged. This was necessary since the mirrors have shown deformations of the Al-plate which was caused by tension due to extension of frozen water inside of the mirror honey comb structure (*popcorn mirrors*). There was no report about the work and since there is still need to exchange further 24 mirrors we would like to summarize our experience in this report.

Figure 16 shows the exchanged mirrors in black color. This figure contains additionally the latest update of the deformed mirror segments on the MAGIC telescope (red and yellow).

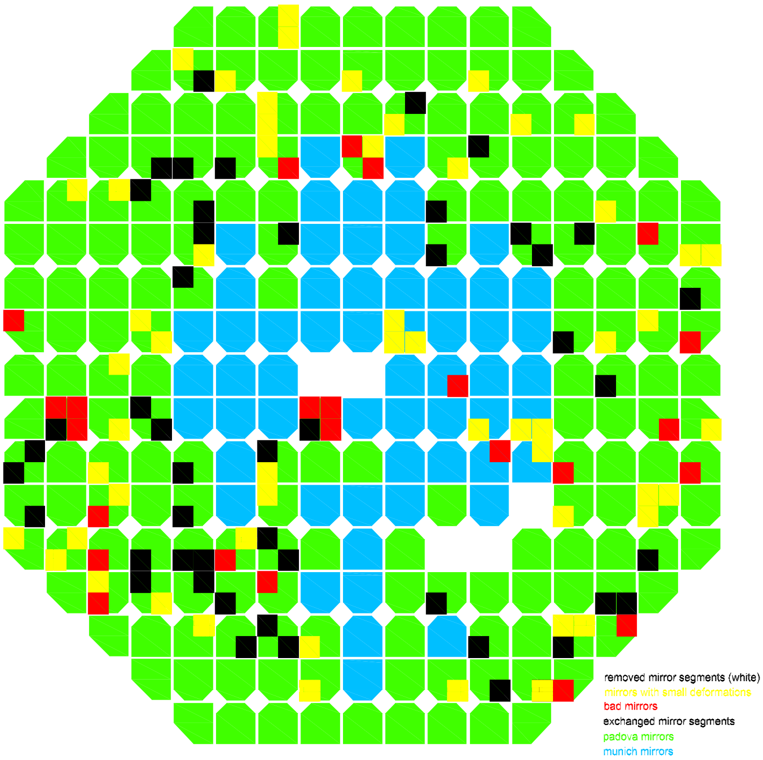

Figure 16: Status of MAGIC mirrors. Mirrors in black have been exchanged in October 2005. Red mirrors show deformations of the mirror surface. Yellow mirrors show less deformations. Three panels are marked white. This panels have been removed from the telescope dish and are already substituted with new 1 m^2 mirrors. There are also four single mirror segments that have been removed.

According to the figure above, 24 mirrors show visible deformations and are marked for exchange in the near future (red color). Additionally 55 mirrors show small deformations (mainly at the borders of the mirror). If this mirrors get worser in the next bad weather period, than we should also replace them (yellow color).

4.1 Experience during mirror replacement

It was the first time we had to exchange an bigger number of mirrors in an short period of time. Since there is still an big amount of bad mirrors (see figure 16) we would like to summarize the experience we gained during the work. Based on this experience we think to be able to improve the work efficiency in the future.

The team working on the mirror replacement should contain at least the three following persons:

Coordinator : This person has to coordinate the work and prepare the next mirrors and provide them to the technicians working on the telescope structure. The mirror segments have to be assembled with three legs which fix them to the panel and with the heating unit.

Cherry picker driver : He has to have much experience moving the cherry picker. Most of the mirrors in the central part of the reflector are only accessible by entering with the cherry picker arm between the wires of the camera bow. The panels of the chess structure which stand out are only accessible from the cherry picker. The driver has to unscrew the nuts from the mirror and remove the mirror. This mirrors are easier to remove than the one in the lower plane of the chess-structure.

Climber : This person has to climb the telescope structure dish behind the mirrors. He has to unplug the heating cables and connect them again after the new mirror was mounted. The mirrors mounted on panels in the back plane of the chess structure (closer to the carbon fiber tubs) are only accessible from the telescope dish. In this case the climber has to unscrew the nuts.

For the next exchange we suggest to organize two teams composed by three persons each. The teams can work in two different shifts. The first one starts at 8:30 and it finishes at 14:00, while the second one starts at 14:00 and it finishes at 19:30. This operative system always guarantees eleven working hours per day and is making use of all day light. In this constellation it will be possible to replace minimum 8 mirrors per day.

Finally, the work has to be coordinated with the data-taking shift crew in order to park the telescope after the shift in the correct position. The mirrors located in the upper part of the telescope dish can only be accessible when the telescope azimuth position is turned over the Zenith ($< -70°$).

References

[1] Goebel F. et al., *Absolute energy scale calibration of the MAGIC telescope using muon images*, Proc. 29th International Cosmic Rays Conference, Pune, India (2005), available on http://wwwmagic.mppmu.mpg.de/publications/conferences/icrc05/goebel_muons.pdf

[2] Meyer M., *Calibration of the MAGIC telescope using muon rings*, MAGIC-TDAS 05-10, Germany (2005)

[3] Würzburg datacenter: http://magic.astro.uni-wuerzburg.de/mars/db/sequinfo.php

[4] Mirzoyan R. et al., *Contraints in Reducing the Threshold of Imaging Cherenkov Telescopes*, Proc. Towards a Major Atmospheric Cherenkov Detector, 298-315 (1997)

[5] Pichler B.J., Lorenz E., Mirzoyan R. et al., *Production of a diffuse very high reflectivity material for light collection in nuclear detectors*, NIM A 442, 333-336 (2000)